Geotectonical Parameters and Seismic Hazard Assessment for GASCO Site, Eastern Desert, Egypt*

Kamal Abdel-Rahman El-Sayed

(Seismology Dept., National Research Institute of Astronomy and Geophysics, Helwan, Cairo, Egypt)

Abstract: GASCO site has been evaluated on the basis of site investigation, seismic activity and seismic hazard assessment. Shallow seismic refraction survey has been carried out to estimate the elastic and dynamic constants for soil and rock materials throughout 8 seismic profiles. The ground model at the site consisting of two layers characterized by moderate to high values of elastic and dynamic constants indicates that the site has good soil and foundation rock. Both historical and instrumental earthquakes in a circle with radius of 150 km around the proposed site were collected and precisely analyzed. The site is affected by four seismic source zones: Central Gulf of Suez, Cairo-Suez District, Southwest Cairo and Beni-Suef, based on the tectonic setting, the seismicity, geological structures and fault plane solutions of major earthquakes. Maximum earthquake moment magnitudes (M_W) have been identified for these source zones using seismicity statistics together with expert judgment. In addition, the stochastic approach was applied for the seismic hazard assessment in terms of Peak Ground Acceleration (PGA) and response spectra. It is noticed that Beni-Suef is the nearest source to the site and the maximum PGA value produced from this seismic source reaches 9.34 cm/s^2. This value is small and reflects that there is no hazardous effect to be expected at GASCO site, which indicates its validity for civil engineering purposes. The response spectra at 1%, 3%, 5% and 10% damped Pseudo-acceleration (PSA) were also simulated at the GASCO site.

Key words: seismic refraction; seismic hazard; site response

CLC number: P315.9 Document code: A Article ID: 1000-0666(2008)02-0160-11

0 Introduction

The Egyptian company for Natural Gases (GASCO) selected a site in the eastern Desert of Egypt to construct an assembly for the natural gases. The estimation of dynamic characteristics for the subsurface ground structure and the seismic hazard assessment for this site became important and necessary. The shallow seismic refraction techniques are considered as one of the accurate and cost-effective methods used in engineering, archaeological and environmental investigations①. Values of P- and S-wave velocities obtained from shallow seismic refraction surveys were used to determine the geotechnical properties for the foundation rock at GASCO site. The produced damage due to earthquake occurrences in different localities all over the world leads to the critical need for evaluation of earthquake activity and the seismic hazard assessment at the proposed sites for strategic projects. The stochastic simulation techniques proposed by Boore [2003] were used for the seismic hazard assessment in terms of Peak Ground Acceleration (PGA) and the response spectra. The prediction of ground motion or response amplitude as a function of earthquake magnitude and distance is of fundamental importance for the assessment of seismic hazard.

1 Geological and Structural Setting

The proposed site is located in the northern part of the Eastern Desert about 38 km east of the Nile River, at 29°04′29″N and 31°28′10″E (Figure 1). Topographically, the site represents a part from the

* Received date: 2007-08-30.

① Burger H R. 1996. Exploration geophysics of the shallow subsurface. Prentice Hall.

Eastern Desert plateau where its elevation ranges from 333 m to 343 m above sea level. Geologically, the site is built mainly with Eocene limestone [Said, 1990]. Structurally, GASCO site is located in the stable shelf zone and there are no major structures encountered at surface of the selected site.

Figure 1. Location map of the proposed GASCO site.

2　Geotechnical Evaluation of the GASCO Site

2.1　Seismic Refraction Survey

Seismic refraction survey for 8 profiles was carried out at the site (Figure 2) using the 24-channel signal enhancement seismograph which was GEOMETRICS Strata View model. Each profile was 240 m long and the distance between two successive geophones was 10 m. The technique (for P-wave generation) is to shoot the profile at 10 m away from each end (normal and reverse shooting) and also from its mid-point for profiles No. 1 to No. 3. While from the profiles No. 4 to No. 8 the shooting was done behind each end with 10 m, at mid-point, at the distances of 65 m (between geophones No. 6 and No. 7) and 180 m (between geophones No. 18 and No. 19). The source of energy was the hydraulic weighting drop with a total mass weight of 100 kg. While the generation of shear waves (SH) was acquired using the horizontal geophones and a slotted striker plate by hitting one end of the plate horizontally using sledgehammer.

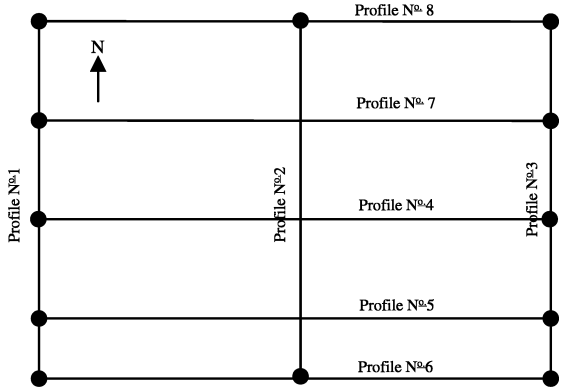

Figure 2. Location of the seismic profiles at Gasco site.

2.2　Data Analysis and Results

The seismic refraction data obtained from GASCO site was processed and analyzed using both SIP and SEISREFA programs which are complete seismic refraction processing and modeling software. The travel time-distance curves and the corresponding 1-D (one-dimension) ground models were obtained (Figure 3).

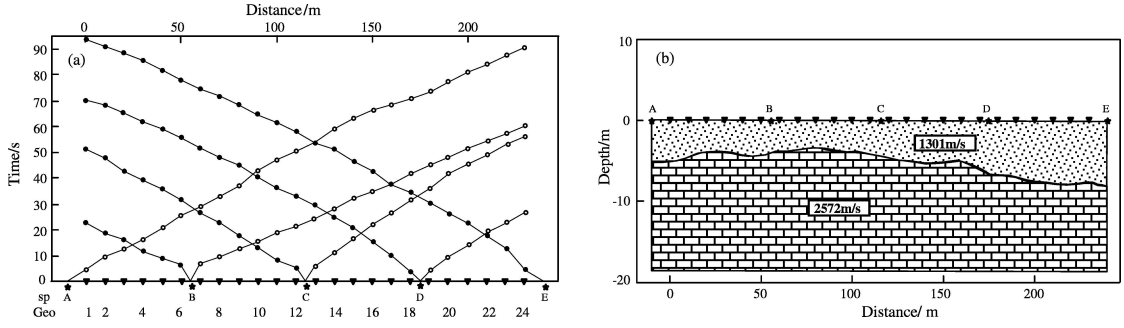

Figure 3. Travel time-distance curve (a) and depth model (b) for profile No. 4.

The elastic properties and the material competence coefficients for the site are deduced (Table 1 and 2) for both surface and second layers. In the tables, the ultimate bearing capacity is indicated by Q_{ult}.

2.3 Elastic properties

The values for both P- and S-wave velocities are used to compute the elastic constants of the detected subsurface layers (Table 1 and 2). These constants include the density (ρ), stress ratio (S_i), Poissons ratio (σ), rigidity modulus (μ), Youngs modulus (E) and Bulks modulus (B) as follows:

(1) Stress Ratio (S_i)

The propagation of seismic waves is proportional to the differential pressure between the sedimentary overburden and the pore-filling fluids. This means that the high fluid pressure formations will have differential pressure and abnormally low seismic wave velocities. According to Abdel Rahman [1989] the stress ratio is given as:

$$S_i = 1 - 2(V_S^2 / V_P^2). \qquad (1)$$

The obtained values of the study area range from 0.349 to 0.397 in the surface layer (Figure 4a) and from 0.202 to 0.391 in the second layer (Figure 4b). These values of stress ratio reflect competent materials at the site.

(2) Poissons Ratio (σ)

This ratio represents the geometrical change in the shape of an elastic body. Its value is 0.5 for fluids and it approaches zero for very hard indurate rocks. Negative Poisson's ratio is also recorded for very hard indurate anisotropic rocks. Poisson's ratio (σ) is given in terms of P- and S-wave velocities [Abdel Rahman, 1992]:

$$\sigma = [(V_P/V_S)^2 - 2]/[(V_P/V_S)^2 - 2]. \qquad (2)$$

The values lie in the range from 0.258 to 0.344 in the surface layer (Figure 5a), and range from 0.168 to 0.281 in the second layer (Figure 5b), which indicate hard rocks. For the surface layer the area of profile No. 3 is of the highest value. But the second layer reflects the area of profile No. 1 is of the highest value.

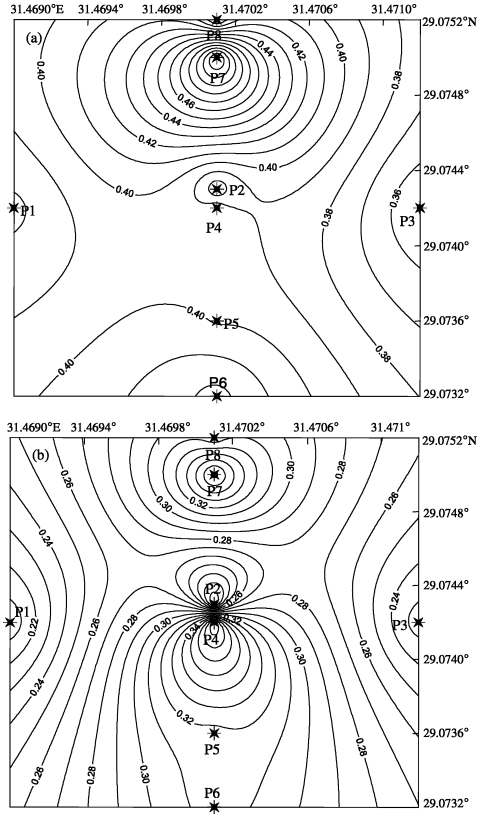

Figure 4. Distribution of stress ratio for the surface layer (a) and second layer (b).

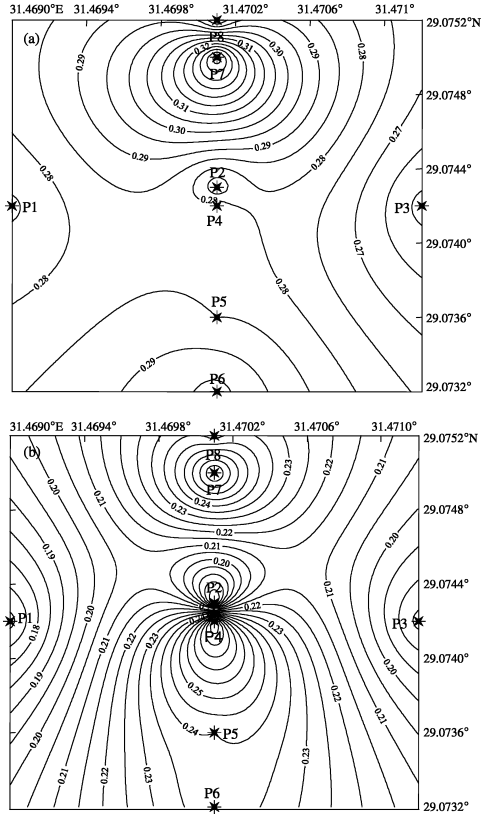

Figure 5. Distribution of Poissons Ratio for the surface layer (a) and second layer (b).

Table 1. Seismic velocities and elastic properties of the surface layer at GASCO site

surface layer Profiles	V_{Pi} /m·s^{-1}	V_{Si} /m·s^{-1}	Density ρ /gm·cm^{-3}	Poisson ratio σ	Rigidity modulus μ/dyn·cm^{-2}	Young's modulus E/dyn·cm^{-2}	Bulk's modulus B/dyn·cm^{-2}	Material Index M_i	Concentration Index C_i	Stress ratio S_i	N-Value	Q_{ult} /kg·cm^{-2}	Ultimate bearing capacity Q /kPa
P1	1 201	670	1.824 935	0.274 082	8.192E+09	2.09E+10	1.538E+10	-0.096 33	4.648 546	0.377 566	361.500 4	10.830 57	1.062 154
P2	1 143	637	1.802 492	0.270 695	8.093E+09	2.064E+10	1.518E+10	-0.082 78	4.690 717	0.371 168	343.695 1	10.297 12	1.009 838
P3	1 357	774	1.881 511	0.258 898	1.127E+10	2.84E+10	1.96E+10	-0.035 59	4.862 518	0.349 343	551.925 6	16.534 4	1.621 528 8
P4	1 301	714	1.861 791	0.284 497	9.491E+09	2.44E+10	1.884E+10	-0.137 99	4.514 975	0.397 618	435.628 1	13.05 098	1.279 909 7
P5	1 033	566	1.757 465	0.285 495	5.63E+09	1.45E+10	1.124E+10	-0.141 98	4.502 689	0.399 57	220.432 1	6.604 771	0.647 729 9
P6	889	477	1.692 728	0.297 857	3.851E+09	1.00E+10	8.234E+09	-0.191 43	4.357 316	0.424 211	133.472 6	3.999 594	0.392 240 2
P7	1 375	670	1.887 719	0.344 318	8.474E+09	2.28E+10	2.437E+10	-0.377 27	3.904 288	0.525 131	361.500 4	10.830 57	1.062 154
P8	1 003	556	1.744 564	0.278 198	5.393E+09	1.38E+10	1.035E+10	-0.112 79	4.594 565	0.385 421	209.205	6.268 437	0.614 745 6

Table 2. Seismic velocities and elastic properties of the second layer at GASCO site

surface layer Profiles	V_{Pi} /m·s^{-1}	V_{Si} /m·s^{-1}	Density ρ /gm·cm^{-3}	Poisson ratio σ	Rigidity modulus μ/dyn·cm^{-2}	Young's modulus E/dyn·cm^{-2}	Bulk's modulus B/dyn·cm^{-2}	Material Index M_i	Concentration Index C_i	Stress ratio S_i	N-Value	Q_{ult} /kg·cm^{-2}	Ultimate bearing capacity Q/kPa
P1	2 065	1 304	2.089 737	0.168 381	3.553E+10	8.30E+10	4.169E+10	0.326 476	6.938 915	0.202 474	2 548.067	76.312 19	7.483 936 1
P2	2 293	1 447	2.145 175	0.172 503	3.648E+10	8.554E+10	4.296E+10	0.309 988	6.797 112	0.208 463	2 827.494	84.680 78	8.304 643
P3	2 811	1 750	2.257 236	0.183 575	6.913E+10	1.64E+11	8.61E+10	0.265 7	6.447 362	0.224 852	6 037.748	180.795 5	17.730 612
P4	2 572	1 419	2.207 646	0.281 212	4.445E+10	1.14E+11	8.668E+10	-0.124 85	4.556 038	0.391 231	3 264.747	97.771 52	9.588 453 3
P5	2 757	1 612	2.246 316	0.240 276	5.837E+10	1.45E+11	9.282E+10	0.038 897	5.161 885	0.316 267	4 745.282	142.100 1	13.935 754
P6	3 057	1 789	2.305 078	0.239 572	7.377E+10	1.83E+11	1.169E+11	0.041 713	5.174 114	0.315 049	6 440.894	192.865	18.914 275
P7	2 553	1 438	2.203 558	0.267 656	4.557E+10	1.16E+11	8.279E+10	-0.070 62	4.736 137	0.365 479	3 394.606	101.659 8	9.969 772 1
P8	2 753	1 626	2.245 501	0.232 137	5.937E+10	1.46E+11	9.094E+10	0.071 451	5.307 795	0.302 316	4 867.155	145.748 9	14.293 599

2.4 Material Competence Coefficients

There are a number of competence scales, based on the values of P- and S-wave velocities and elastic moduli in consequence, which are used to evaluate the soundness of rocks or soil materials, including the material index (M_i), concentration index (C_i), N-value and ultimate bearing capacity (Q_{ult}) as follows:

(1) Material Index (M_i)

Material index (M_i) is defined as the degree of competence of the material on the basis of the elastic moduli. This index must have relation with the material composition, the degree of consolidation, fracturing and jointing, the presence or absence of fluids in pore spaces which affect the elastic moduli. The material index is given [Abdel Rahman, 1989] as follows:

$$M_i = (1-4\sigma). \quad (3)$$

Where σ is the Poisson's ratio. The values range between −0.377 and −0.035 in the surface layer (Figure 6a), while they range from −0.124 and 0.326 in the second layer (Figure 6b), and they indicate hard rocks. For the surface layer the area of Profile No. 3 is of the highest value. But for the second layer the area of Profile No. 1 is of the highest value.

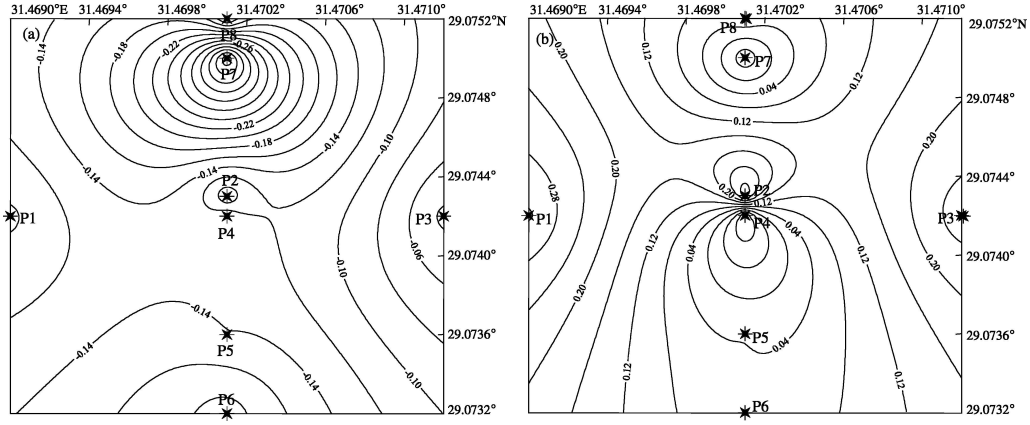

Figure 6. Distribution of Material Index for the surface layer (a) and second layer (b).

(2) Concentration Index (C_i)

The concentration index (C_i) describes the degree of material concentration. The soil compaction status is considered, to a great extent, as a measure of the degree of competence for foundation and other civil engineering purposes. It depends on both elastic moduli of the soil and the pressure distribution at their depth. The concentration index can be given in terms of velocity squared ratio [Abdel Rahman, 1989] as:

$$C_i = (3-4\alpha)/(1-2\alpha). \quad (4)$$

Where α is the velocity squared ratio (V_S^2/V_P^2). The obtained values in the surface layer ranges from 3.904 to 4.862 (Figure 7a) and from 4.736 to

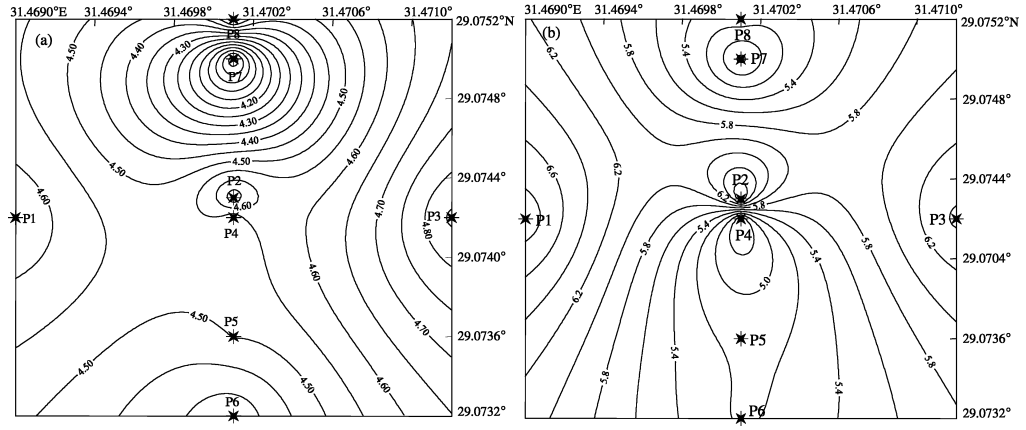

Figure 7. Distribution of Concentration Index for the surface layer (a) and second layer (b).

6.938 in the second layer (Figure 7b). This means that area of profile No. 3 has the highest values for the surface layer, while the area of profile No. 1 is of the highest values for the second layer.

(3) The N-value

This value is the resistance to penetration by normalized cylindrical bars under standard load, which is geophysically known as the Standard Penetration Test (SPT). N-value can be evaluated using the following formula [Imai et al., 1976; Stuempel et al., 1984]:

$$V_S = 89.9 \times N^{0.341}. \quad (5)$$

Where V_S is the horizontal shear wave velocity. Material having low N-value indicates soft soil. The high values (between 133 and 551) in the surface layer (Figure 8) indicate a compacted soil at the site and hence there is no need to calculate the N-values for the second layer.

(4) Ultimate Bearing Capacity (Q_{ult})

The natural and the artificial cyclic dynamic loading create additional load which is added to the building load and may cause soil liquefaction if the total loading value exceeds the ultimate bearing capacity (Q_{ult}) of the material①. Q_{ult} can be given in terms of shear wave velocity [Abdel Rahman et al., 1992] as:

$$\lg Q_{ult} = 2.932(\lg V_S - 1.45). \quad (6)$$

The obtained values range between 3.99 and 16.534 kg/cm^2 in the surface layer (Figure 9a) and from 76.312 to 192.862 kg/cm^2 (Figure 9b) in the second layer. These values reflect that the area of profile No. 3 is of the highest values for the surface and second layers.

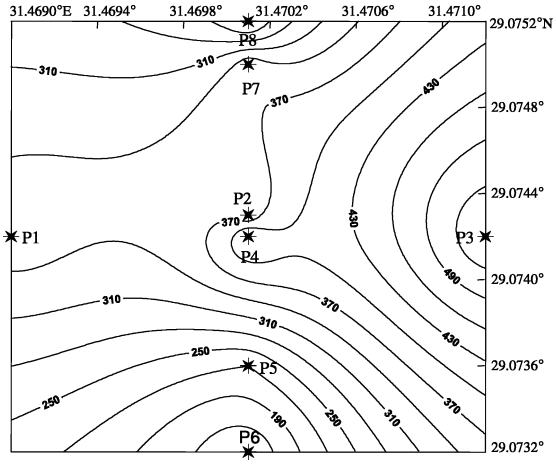

Figure 8. Distribution of N-value for the surface layer.

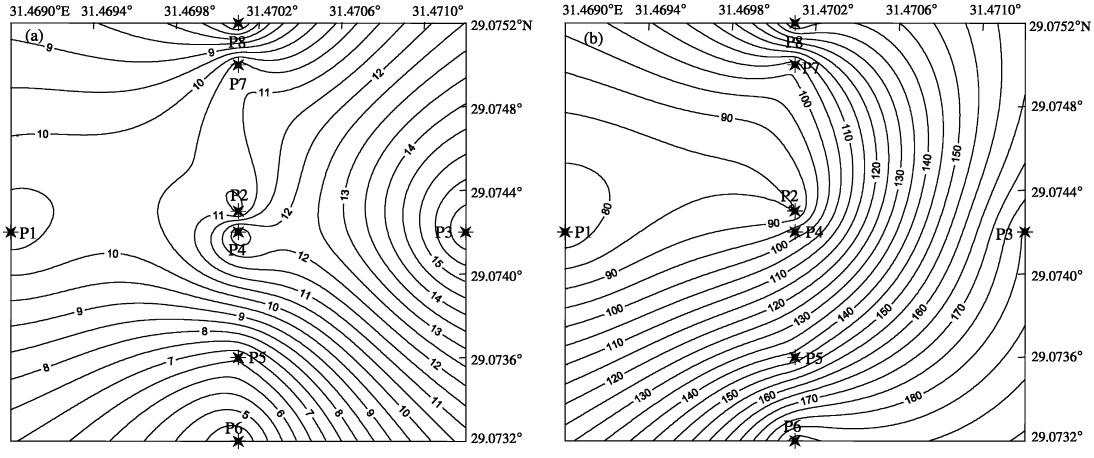

Figure 9. Distribution of Q_{ult} for the surface layer (a) and second layer (b).

3 Seismic Hazard Assessment for GASCO Site

3.1 Earthquake Activity

The available earthquake data around GASCO site contain two types of information: historical observations (pre-1900) of major seismic events that occurred over a period of about 4,000 years and instrumental earthquakes (1900—July 1997) that collected from Maamoun et al. [1984], Ambraseys et

① Bowels J E. 1984. Physical and geotechnical properties of soils. McGrew-Hill, London.

al. [1994] and International Seismological Center (ISC). Data from Aug. 1997 till Dec. 2004 were gathered from the Bulletins of the Egyptian National Seismological Network (ENSN). From the distribution of the earthquake activity around the GASCO site (Figure 10) it is noticed that GASCO site is located in the mainland of the eastern desert and surrounded by the earthquakes with magnitude ranging from less than 3 to greater than 5.

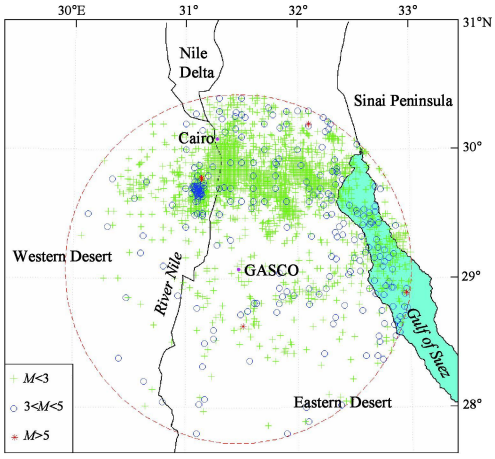

Figure 10. Earthquake activity in a 150-km circle around GASCO site.

3.2 Seismic Source Zones

The definition of seismic zones carried out in the present work depends on historical and instrumental earthquakes as well as the results of the previous geophysical and geological studies including the kind of seismic faulting [Papazachos et al., 1984], seismicity rate (a-value) [Papazachos, 1980], b values [Hatzidimitriou et al., 1985], major trends of geological zones [Mountrakis et al., 1983], and the fault plane solutions of the major earthquakes (i.e. strike, dip and stress axes). A seismic zone is a configuration within which it is assumed that an earthquake recurrence process is considered to be spatially and temporally homogeneous. The delineation of the seismotectonic sources usually represents the major part of any seismic hazard analysis. According to this study the seismic activities are concentrated in 4 seismic zones as follows: Central Gulf of Suez zone, Cairo-Suez District zone, Southwest Cairo zone, Beni-Suef zone.

3.2.1 Central Gulf of Suez zone

Fault plane solutions show the mixing between the earthquakes occurred on the marginal faults and those occurred on the transverse ones. Also, some of them are nearly of a pure normal faulting, while the others have a considerable strike-slip component [Maamoun et al., 1984].

The central Gulf of Suez zone has a regional northeast dip and bounded from north and south by 2 major accommodation zones of relatively flatter dip separating it from both the northern and southern provinces. Geophysical and geological observations confirm this model. The seismic activity in the central provinces is low compared with both the southern and northern provinces. This becomes clear after the establishment of ENSN.

3.2.2 Cairo-Suez District zone

It is located in the northeastern Desert and extends from Cairo to Suez at the north of the Gulf of Suez. It is characterized by small to moderate earthquakes. The Cairo-Suez district is affected by 3 fault trends. One of them is the E-W trend, mostly pronounced and almost aligned by latitude 30°N, where the other 2 trends (ENE and NW) are spatially more dispersed [Abdel-Rahman et al., 1978]. The focal mechanism for the 1974 Abu-Hammed earthquake① [Mousa, 1989] shows two planes trending ENE-WSW and NNW-SSE with left-lateral strike-slip motion along the second plane. The focal mechanism of 1984 Wadi-Hagul earthquake shows the same strike-slip with reverse component. In addition, the mechanism of the 1987 Ismailiya earthquake shows strike-slip also with two nodal planes trending N68°E and S24°E with steep dip angles (80° and 80°)②.

① Hassib G H. 1990. A study of focal mechanism for recent earthquakes in Egypt and their tectonic implication. Egypt: Fac. of Sci., Assiut Univ., Egypt.

② Megahed A., Dessoky M M. 1988. The Ismailia (Egypt) earthquake of January 2nd 1987 (Location, Macroseismic Survey, Radiation pattern of first motion and its tectonic implications).

3.2.3 Southwest Cairo zone

This zone was defined depending on the epicentral distribution, seismicity level, and the a-value which is determined for this zone (a=3.07). The focal mechanisms of some earthquakes in this zone show a normal faulting only or a normal faulting with large strike-slip component[Abu El-Enean, 1997]. The first nodal plane is trending nearly E-W (WNW-ESE) parallel to the Mediterranean trend. This shows the coincidence with the surface lineaments, as appeared directly after the occurrence of the 1992 earthquake and the general tectonics of the area. Therefore, this plane is recommended to be the most probable fault plane. The auxiliary plane is trending mainly NW-SE parallel to the Gulf of Suez. NoNE-SW trend parallel to the Pelusium trend is given by the focal mechanisms.

3.2.4 Beni-Suef zone

Beni-Suef zone is located to the east of the Nile Valley. Meshref[1982] indicated that the basic tectonic trends affecting northeast Africa are WNW and ENE. Halsay① considered the N60°W trend is the significant trend in northern Egypt. This zone has a tentative trend parallel to the Red Sea trend from the distribution of earthquake epicenters. The parameter a-value is 1.49. The focal mechanism for Beni Suef earthquake on 11 October 1999 indicates a normal faulting mechanism with minor horizontal movement with trends NW-SE and ENE-WSW [Abu El Enean at al, 2003].

3.2.5 Maximum Earthquake Magnitude

This step requires a determination of the maximum earthquake for each of the identified seismotectonic sources. In deterministic analysis it is more common to define the maximum earthquake as a maximum credible earthquake [Reiter, 1991]. Another kind of maximum earthquake is the maximum historic earthquake with increasing 0.5 units. There are 4 seismic source zones affecting the site and each of them has its own seismic activity.

The earthquake activity in terms of focal depth and horizontal axes together with the later activity are used to determine the dimensions of the active seismic source area [Abu-Elenean, 1997]. The epicentral distribution of the seismic activity of the southwest Cairo seismic zone indicates that the maximum dimension of the activity is 41 km and the depth ranges from 7 to 25 km yielding a thickness of a seismogenic layer of 18 km. Thus the total seismogenic area of this zone is 738 km². According to Papazachos et al. [2004], the maximum earthquake of this zone is found to be with moment magnitude 6.31.

Using the same techniques for the central Gulf of Suez, the expected maximum earthquakes are determined, while the historical approach was used for the other seismic sources (Table 3).

Table 3 Maximum expected magnitude and hypocentral distances from each seismic source to GASCO site

Seismic Source	Maximum magnitude	Hypocentral distance to the site/km
Central Gulf of Suez Zone	5.5	139
Cairo-Suez Zone	5.4	170
Southwestern Cairo Zone	6.31	84
Beni-Suef Zone	5.6	48

3.3 Simulation of Ground Motion at GASCO Site Using Stochastic Method

3.3.1 Input Parameters

(1) The source parameters[E(M0, f)]

The earthquake source spectrum E(M0, f) for the horizontal component of ground motion is given by the following:

$$E(M_0, f) = C(2\pi f)^2 M_0 S(M_0, f). \quad (7)$$

where S(M0, f) is the displacement source spectrum and C is a constant. $C = R_{\theta} VF/(4\pi\rho\beta^3 R)$, with R= 1 km, R_{θ}=0.55 (average shear wave radiation pattern), F=2.0 (free surface effect), V=0.71 (partition onto two horizontal components), ρ is the density at the source and β is the shear wave velocity at the source.

(2) The path[P(R, f), duration]

In this study the three-segment geometrical spreading operator of Atkinson et al. [1995] is

① Halsay J. 1975. Interpretation of ERTS linears. Cairo: Cairo University.

used. Geometrical spreading R^{-1} is assumed for distance less than 70 km and $R^{0.0}$ for distances from 70 km to 130 km and $R^{-0.5}$ for greater distances. The Q model derived by Moustafa [2002] is used to represent the anelastic attenuation factor. This model is represented as:

$$Q = 85.68 f^{0.79}. \quad (8)$$

Although the Fourier spectrum of ground motion is not dependent on the duration, duration is a very important parameter for peak motions decrease with increasing duration. The duration is a function of the path, as well as the source:

$$T = T_0 + bR \quad (9)$$

Where T_0 is the source duration and bR represents the path dependent term that accounts for dispersion. Following Hanks et al. [1981], the source duration is related to the corner frequency by

$$T_0 = f^{-1}. \quad (10)$$

Empirical observations and theoretical simulations suggest that the path-dependent part of the duration can be represented by a connected series of straight line segments with different slopes. The function of Atkinson et al. [1995] is used where the path duration is modeled as trilinear using the transition distances 70 and 130 km for consistency with the attenuation model. The slope is 0.16 for the distance ranges between 10 and 70 km, −0.03 for the distance ranges between 70 and 130 km and 0.04 for the distance ranges from 130 to 1,000 km. The slope is assumed to be zero for the distances less than 10 km.

(3) The site $G(f)$

The factors that control the change of the seismic ground motion amplitudes at the earth's surface are impedance and diminution. Boore [2003] separated the path effect $G(f)$ into two terms as follows:

$$G(f) = A(f) + D(f). \quad (11)$$

Velocity and density model is converted into site amplification $A(f)$, using the square root of the impedance ratio between the source and the surface. For polarized shear waves, the impedance is defined as the product of the shear wave velocity, density and the cosine of the angle of incidence. The amplification is relative to the surface motion that would exist if the material were replaced with uniform material whose velocity and density equal to those at the source.

3.3.2 Results

It is noticed that Beni-Suef seismic zone represents the nearest seismic zone to the proposed site (Table 3) and by application of stochastic simulation method, the peak ground acceleration at the site has obtained (Table 4). The simulated time history of PGA, velocity and displacement at the GASCO site for Beni-Suef seismic zones was calculated (Figure 11).

Table 4 Maximum PGA at the site for two seismic zones

Seismic zone	Max magnitude (M_W)	Max PGA/cm·s^{-2}
Southwest Cairo	6.31	2.55
Beni-Suef	5.6	9.34

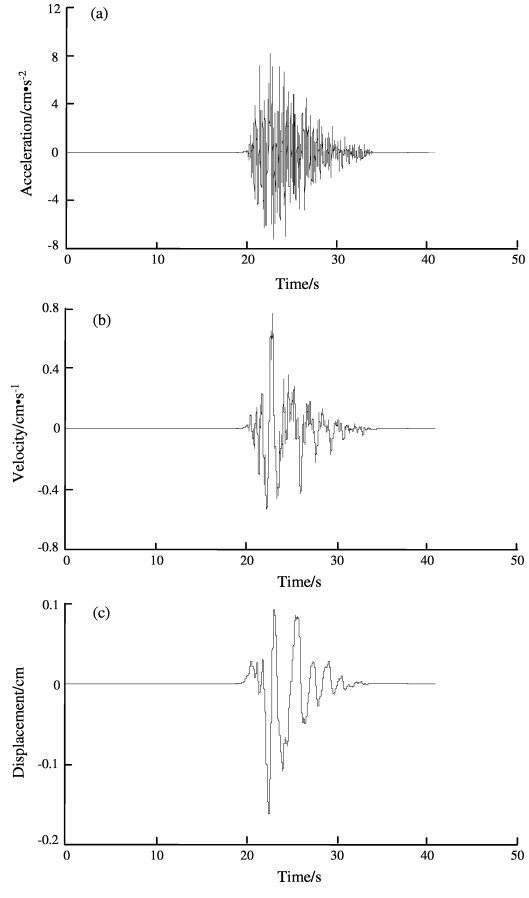

Figure 11. Simulated time history of the maximum PGA, PGV and PGD at GASCO site for Beni-Suef zone

3.3.3 Response Spectra

Response spectra are defined on the basis of the response of single degree of freedom damped oscillator to the earthquake acceleration[Jennings, 1983]. The response spectra of an accelerogram serve the dual function characterizing the ground motion as a function of frequency and providing a tool for determining earthquake resistant design criteria. The response spectra were calculated with four selected damping values of 1%, 3%, 5% and 10% of the critical damping at GASCO site for Beni-Suef zone (Figure 12).

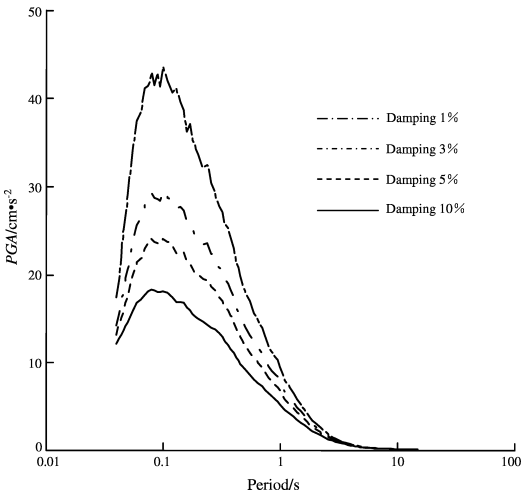

Figure 12. Response spectra for maximum PGA at GASCO site for Beni-Suef zone.

4 Conclusions

Eight seismic profiles are carried out at GASCO site. It is noticed that the ground model consists of two layers. Both elastic moduli and material competence scales have been calculated and indicate that the site has a good soil and hard limestone rock. The seismic activity in a 150-km-radius circle has been collected from different data sources. Four seismic source zone which may affect GASCO site were identified and the maximum expected moment magnitudes were estimated for each seismic source zone. The stochastic technique was used for the simulation of the time history and response spectra for the PGA at GASCO site. Beni-Suef zone represents the nearest seismic source zone to GASCO site and the seismic moment of maximum earthquake that occurs from this source is found to be 2.82×10^{24} dyn·cm. The simulated PGA is about 9.34 Gal. Based on this study it can be concluded that GASCO site is characterized by its low seismic activity and low values of PGA. In addition, the response spectra at GASCO site are calculated and available. This indicates that the selected site is valid and safe for construction purposes.

References

Abd El Rahman M. 1989. Evaluation of the kinetic moduli of the surface materials and application to engineering geologic maps at Ma'Barrisabah area (Dhamar province), Northern Yemen [J]. Egypt J geol, 33 (1—2): 229—250.

Abdel-Rahman M A, El-Etr H A. 1978. The orientational characteristics of the structure grain of the Eastern Desert of Egypt[C] // International Symp. on Evolution and Mineralization of the Arabian-Nubian Shield. Inst. Appl. Geol. Jeddah, S. A.

Abd El Rahman, M. Setto I and El Werr A. 1992. Inferring mechanical properties of the foundation materials at the 2nd Industrial zone [C] // City geophysical measurements E. G. S. Proc. of the 10th Ann. Meet. 50—61.

Abu El-Enean K. 1997. A study on the seismotectonics of Egypt in relation to the Mediterranean and Red Sea tectonics[D]. Cairo: Ain Shams Univ., Cairo.

Abu El Enean K, Deif A. 2003. Seismological Aspects and Source parameters of Beni-Suef earthquake on 11 October 1999 [J]. Bull. Fac. of Sci., Cairo Univ., 71: 27—47.

Ambraseys N N, Melville C P, Adams R D. 1994. The seismicity of Egypt, Arabia and the Red Sea[G] // A historical review. Cambridge: Cambridge Univ. Press: 181.

Atkinson G M, Boore D M. 1995. Ground motion relations for eastern North America[J]. BSSA, 85 (1): 17—30.

Boore D M. 2003. Simulation of ground motion using the stochastic method[J]. Pure and Applied Geophysics, 160 (3—4): 635—676.

Hanks T C, McGuire R K. 1981. The character of high-frequency strong ground motion[J]. BSSA, 71 (6): 2071—2095.

Hatzidimitriou P M, Papadimitrio E E, Mountrakis D M, et al. 1985. The Seismic Parameter b of the frequency-magnitude relation and its association with the geologic zones in the area of Greece[J]. Tectonophysics, 120: 141—151.

Imai T, Fumoto H, Yokota K. 1976. P- and S-wave velocities in subsurface layer of ground in Japan[R]. Tokyo: Urawa Research Institute, Tokyo.

Jennings P C. 1983. Engineering seismology [C] // Kanamori H, Boschi E. Proceedings of the International School of Physics "Enrico Fermi". Course LXXXV: 138—173.

Maamoun M, Megahed A, Allam A. 1984. Seismicity of Egypt[J].

Bull. HIAG, Ⅳ (Ser. B): 109—160.

Meshref W. M. 1982. Regional structural setting of northern Egypt [C] // 6th Explor. Seminar. Egyptian General Petroleum Corporation. Cairo, Egypt: 22.

Moustafa S. 2002. Assessment of ground motion variation for seismic hazard mitigation in the vicinity of Cairo metropolitan area [D]. Ain Shams Univ.

Mountrakis D., Sapountzis E., Kilias A., et al. 1983. Paleogeographic conditions in the western Pelagonian margin in Greece during the intial rifting of the continental area [J]. Can. J. Earth Sci., 20: 1673—1681.

Mousa H. M. 1989. Earthquake activities in Egypt and adjacent regions and its relation to geotectonic features in A. R. Egypt [D]. Mansoura University.

Papazachos B. C. 1980. Seismicity rates and long-term earthquake prediction in the Agean area [J]. Quaternjones Geodaesiae, 3: 171—190.

Papazachos B. C., Kiratzi A. A., Hatzidimitriou P. M. 1984. Seismic faults in the Agean area [J]. Tectonophysics, 106: 71—85.

Papazachos B. C., Scordilis E. M., Panagiotopoulos D. G., et al. 2004. Global relations between seismic fault parameters and moment magnitude of Earthquakes [J]. Bull. Geol. Soc. Greece, XXXVI: 1482—1489.

Reiter L. 1991. Earthquakes hazard analysis [M]. New York: Columbia Univ. Press.

Said R. 1990. Geology of Egypt [M]. Amesterdam: Elsevier Publication.

Stumpel H., Kaehler S., Meissner R., et al. 1984. The use of seismic shear waves and compressional waves for lithological problems of shallow sediments [J]. Geophysical Prospecting, 32: 662—675.

埃及东部沙漠 Gasco天然气公司工程场地大地构造参数和地震灾害评估

Kamal Abdel-Rahman El-Sayed

(埃及国家天文和地球物理研究所地震学室, 埃及开罗市 Helwan镇)

摘要: 根据埃及 Gasco天然气公司工程场地的现场调查资料、地震活动性和地震灾害评估结果, 对该场地进行了评估。通过浅源地震波折射勘探, 对 8个地震剖面上的土壤和岩石的弹性动态常数进行了分析。场地地面模型包括两层, 分析表明它们具有从中值到高值的弹性动态常数, 说明场地有良好的土壤条件和基岩岩性。同时, 我们搜集和分析了研究区周围 150 km半径范围内的历史和仪器记录地震, 从构造环境、地震活动性、地质构造和主要地震的断层面解等方面进行了研究, 认为场地受 4个震源区的影响: 苏伊士中部海湾、开罗—苏伊士地区、开罗西南和 Beni-Sue地区。我们采用地震活动性统计方法并结合专家判定, 确定了这些震源区内最大地震的矩震级 (M_W)。另外, 依据场地峰值加速度 (PGA) 和反应谱, 用随机方法对场地进行了地震灾害评估。4个震源区中, Beni-Sue地区距离工程场地最近, 其 PGA最大值为 9.34 cm/s², 但这个值很小, 表明地震不会对工程场地产生破坏性影响。最后, 我们还模拟了阻尼为 1%、3%和 5%时的伪加速度场地反应谱。

关键词: 地震折射; 地震破坏; 场地响应

毛先进　云南省地震局正研级高级工程师。1997年毕业于中南工业大学地质系应用地球物理专业，获博士学位。主要从事工程地球物理勘探及地震电磁学研究。

Kamal Abdel-Rahman El-Sayed 埃及国家天文和地球物理研究所地震学室副研究员。分别于1999、1994、1990年毕业于 Zagazig 大学，并获工程地震学博士学位、地质学硕士学位和地球物理学学士学位。现主要从事场地效应评估、地震灾害评估和强震动数据的工程应用研究。

李志祥　云南省地震局地震工程研究院高级工程师。1991年毕业于北京大学地震地质专业。现主要从事建筑工程检测及水库地震监测台网建设工程设计工作，承担“复杂构造区水库地震监测预警研究”运用方面的子课题研究工作。

王　琼　新疆维吾尔自治区地震局副研究员。1997年毕业于新疆师范大学地理专业，获学士学位；2000年毕业于中国地震局兰州地震研究所固体地球物理专业，获硕士学位。主要从事地震预报和应力触发等方面的研究。

张卫东　广州航海高等专科学校交通建筑工程系副教授，一级注册结构工程师。2001年毕业于哈尔滨工业大学结构工程专业，获硕士学位。主要从事土—结构相互作用，工程结构抗震、隔震，差异沉降对上部结构的影响及防控等方面的研究及土木工程的教学工作。

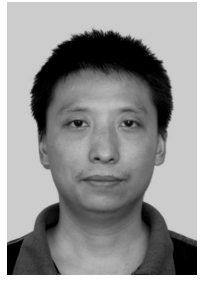

皇　民　河南工程学院讲师。1996年毕业于西安矿业学院建筑工程系，获学士学位；现为西南交通大学土木学院博士研究生。研究方向为地下结构动力分析及抗减震研究。

王曰风　河北省地震局张家口中心台工程师。1999年毕业于石家庄经济学院（原河北地质学院）水文地质与工程地质专业，获学士学位；现为中国科学技术大学固体地球物理专业在读硕士研究生。主要从事地震观测与地震分析预报工作。

史　榕　2005年毕业于吉林大学地球探测科学与技术学院，获硕士学位；现为同济大学海洋与地球科学学院固体地球物理专业在读博士研究生。主要从事 GPS与遥感图像处理方面的工作。